ELSEVIER

Journal of Fluids and Structures 25 (2009) 918–935

JOURNAL OF FLUIDS AND STRUCTURES

www.elsevier.com/locate/jfs

Aeroelastic coupling of geometrically nonlinear structures and linear unsteady aerodynamics: Two formulations

L. Demasi[a], E. Livne[b,*]

[a]*Department of Aerospace Engineering and Engineering Mechanics, San Diego State University, San Diego, CA 92182-1308, USA*
[b]*Department of Aeronautics and Astronautics, BOX 352400, University of Washington, Seattle, WA 98195-2400, USA*

Received 16 July 2008; accepted 21 March 2009

Abstract

Two different time domain formulations of integrating commonly used frequency-domain unsteady aerodynamic models based on a modal approach with full order finite element models for structures with geometric nonlinearities are presented. Both approaches are tailored to flight vehicle configurations where geometric stiffness effects are important but where deformations are moderate, flow is attached, and linear unsteady aerodynamic modeling is adequate, such as low aspect ratio wings or joined-wing and strut-braced wings at small to moderate angles of attack. Results obtained using the two approaches are compared using both planar and non-planar wing configurations. Sub-critical and post-flutter speeds are considered. It is demonstrated that the two methods lead to the same steady solution for the sub-critical case after the transients subside. It is also shown that the two methods predict the amplitude and frequency of limit cycle oscillation (when present) with the same accuracy.

Keywords: Nonlinear aeroelasticity; Transient analysis; Newmark method; Newton–Raphson method; Unsteady aerodynamics; Flutter; Delta wing; Joined wing

1. Introduction

Nonlinear aeroelastic problems involving geometric structural nonlinearities (Hodges, 2006; Friedmann and Hodges, 2003; Tang and Dowell, 1996; Patil and Hodges, 2004) have been the subject of research and development for years, motivated by such aeroelastic systems as helicopter rotors, high-aspect-ratio gliders, and human-powered vehicles. More recently, emerging interest in high-altitude long-endurance (HALE) configurations as well as unconventional configurations such as joined wings (JW) and strut-braced wings has led to a surge in new analysis/computational tools development for such configurations and an effort to understand their aeroelastic behavior and corresponding design and certification issues (Livne and Weisshaar, 2003; Patil et al., 2000; Sulaeman et al., 2002; Livne, 2001; Lee and Chen, 2004). Computational Fluid Dynamics/Computational Structural Mechanics (CFD/CSM) simulation technology is now becoming powerful and efficient enough to begin making its impact on the actual design and certification of flight vehicles (Geuzaine et al., 2003). While general in its formulation, allowing the capture in simulation of both structural and aerodynamic nonlinear behavior, CFD/CSM model preparation and computation are still expensive, requiring

*Corresponding author. Tel.: +1 206 5436643; fax: +1 206 5430217.
E-mail addresses: ldemasi@mail.sdsu.edu (L. Demasi), eli@aa.washington.edu (E. Livne).

0889-9746/$ - see front matter © 2009 Elsevier Ltd. All rights reserved.
doi:10.1016/j.jfluidstructs.2009.03.001

Nomenclature

a_0, a_1, a_2, a_3 parameters used in the time integration (Eq. (41))
a_4, a_5, a_6, a_7 parameters used in the time integration (Eq. (41))
$\mathcal{A}_{\text{full}}$ generalized aerodynamic matrix corresponding to the full order structural finite element model
$\mathcal{A}$ generalized aerodynamic matrix corresponding to the reduced order aerodynamic model
$\mathcal{A}_0$, $\mathcal{A}_1$, $\mathcal{A}_2$ Roger matrices of the reduced order aerodynamic model
$\mathcal{A}_{2+i}$ Roger matrices (lag contributions) of the reduced order aerodynamic model
$\mathcal{A}_0^\star$, $\mathcal{A}_1^\star$, $\mathcal{A}_2^\star$ Roger matrices after the transformation to the full order is applied
$\mathcal{A}_{2+i}^\star$ Roger matrices (lag contributions) after the transformation to the full order is applied
$\mathcal{A}^\star$ full order aerodynamic matrix defined in Eq. (9)
b semi-chord used in the definition of the reduced frequency
B_i, $B_i^\star$ combinations of lag terms (Eq. (27))
$\boldsymbol{C}_D$ damping matrix
$\boldsymbol{C}_i$, $\boldsymbol{C}_i^\star$ combinations of full order lag matrices (Eq. (27))
E elastic modulus
$\boldsymbol{F}_{\text{int}}$ vector containing the internal forces
h thickness of the plate
i index
j complex unit
k ratio between ω and V_∞
$k^\star$ reduced frequency
$k^\star_{\max}$ maximum reduced frequency used in the Roger fit
$[\boldsymbol{K}_G^e]^{\text{shell}}_{\text{TOTAL}}$ geometric stiffness matrix at element level
$\mathcal{K}^{1\ \text{system}}_{T_i\ \text{aero}}$ first lag aerodynamic tangent matrix (see Eqs. (35) and (36))
$\mathcal{K}^{2\ \text{system}}_{T_i\ \text{aero}}$ second lag aerodynamic tangent matrix (see Eqs. (35) and (36))
$\mathcal{K}^\star_{T_{\text{aero}}}$ aerodynamic tangent matrix after the static condensation is performed (see Eq. (39))
$\boldsymbol{K}_T$ structural tangent matrix (see Eq. (36))
$\boldsymbol{K}_{T\,\text{eff}}$ effective stiffness matrix (see Eqs. (35) and (36))
$\boldsymbol{K}^{\text{system}}_{T_{\text{dyn}}}$ dynamic contribution to the effective stiffness matrix (see Eq. (36))
$\boldsymbol{K}^{\text{system}}_{T_{\text{aero}}}$ aerodynamic contribution to the effective stiffness matrix (see Eq. (36))
$\boldsymbol{L}_{\text{unsteady}}$ unsteady aerodynamic force vector
$\boldsymbol{M}$ mass matrix
n iteration ID within a time step
$N_{\text{time step}}$ parameter assigned to define the size of the time step (see Eq. (40))
N_{lag} number of lag terms used in the Roger procedure
$\boldsymbol{P}_{\text{ext}}$ vector containing the non-aerodynamic forces
$\mathcal{P}_{i\,\text{aero}}$ lag aerodynamic force vector (see Eqs. (35) and (36))
$\boldsymbol{P}_{\text{eff}}$ effective force vector (see Eqs. (35) and (36))
$\boldsymbol{P}_{\text{dyn}}$ dynamic contribution to the effective force vector (see Eq. (36))
$\boldsymbol{P}_{\text{aero}}$ aerodynamic contribution to the effective force vector (see Eq. (36))
$\mathcal{P}^\star_{\text{aero}}$ aerodynamic force vector after the static condensation is performed (see Eq. (39))
$\boldsymbol{q}$ vector containing the generalized coordinates
$\mathscr{R}$ number of shape vectors
s Laplace variable
t time
$\boldsymbol{T}$ transformation matrix
$\boldsymbol{u}$ displacement vector referred to the coordinates at the beginning of the current iteration
$\boldsymbol{U}$ cumulative displacement vector
u_x displacement in the x direction
u_y displacement in the y direction
u_z displacement in the z direction
V_∞ freestream velocity
x, y, z coordinate system
$\boldsymbol{x}^{\text{pert}}$ vector containing the coordinates of the nodes of the perturbed configuration
$\overline{\boldsymbol{x}}^{\text{pert}}$ augmented vector obtained from $\boldsymbol{x}^{\text{pert}}$
$\boldsymbol{x}^{\alpha=0}$ vector containing the coordinates of the nodes of the reference configuration
$\overline{\boldsymbol{x}}^{\alpha=0}$ augmented vector obtained from $\boldsymbol{x}^{\alpha=0}$
${}^t[\star]$ quantity $[\star]$ calculated at time t
${}^{t+\Delta t}[\star]$ quantity $[\star]$ calculated at time $t+\Delta t$
${}^0[\star]$ quantity $[\star]$ calculated at time $t=0$ (initial condition)
$[\star]^n$ quantity $[\star]$ calculated at iteration n of a time step
$[\dot{\star}]$ first time derivative of quantity $[\star]$
$[\ddot{\star}]$ second time derivative of quantity $[\star]$

Greek symbols

α angle of attack, Newmark parameter ($\alpha = 1/4$)
β_i generic lag term
$\overline{\beta}_i$ generic lag term multiplied by the ratio between the speed and the semi-chord
δ Newmark parameter ($\delta = 1/2$)
Δt time step

ζ_i	viscous damping ratio	$\boldsymbol{\Psi}$	matrix containing the shape vectors
$\boldsymbol{\mu}_i$	lag state variable	ω	circular frequency
ρ_∞	air density		
ρ	material density	*Subscript*	
τ	dummy variable used in the calculation of the time domain integrals	nd	auxiliary quantity used in the time domain simulation (see Eqs. (32) and (34))
υ	Poisson's ratio		

significant resources. Practically all of the nonlinear aeroelastic simulation approaches to HALE, gliders, and human-powered vehicles to date are based on nonlinear beam models integrated with various levels of unsteady aerodynamic modeling, from essentially two-D strip methods, through panel, and up to CFD methods.

There is a class of nonlinear aeroelastic configurations where nonlinear beam models cannot capture the nonlinear structural behavior, especially localized behavior, in sufficient detail. The aerodynamic behavior of such configurations, however, can be adequately captured by linear unsteady aerodynamic models of the types used for aeroelastic design and certification of practically all modern airplanes, namely, lifting surface and other panel methods as well as linearized CFD models about reference configuration shapes. Such configurations include joined-wings and strut-braced wings operating at high subsonic speeds and attached linear flow, or supersonic configurations in subsonic and supersonic flight, using joined and strut wing concepts together with low-aspect-ratio lifting surfaces (Tang et al., 1999; Attar et al., 2005). Additional cases for which nonlinear structural modeling coupled with linear aerodynamics is adequate involve local structural damage that can lead to local buckling, approach to buckling, or any damage-related geometrically nonlinear behavior of spar and rib areas, cover skins, or substructure joint areas.

Linear steady and unsteady aerodynamic modeling methods of the doublet lattice type (e.g., Doublet Lattice Method (DLM)) or a variety of panel methods for lifting surface/body configurations in subsonic, supersonic, and even hypersonic flow have been the backbone of aeroelastic analysis, design, and certification for years and are still widely used in industry, which accumulated significant experience in their utilization (Rodden et al., 1998). Such methods require model preparation efforts and computer resources that are much less demanding than emerging CFD-based unsteady aerodynamic methods. In a previous paper (Demasi and Livne, 2009, 2007a) we presented one technique for coupling standard linear aerodynamic models with nonlinear structural finite element (FE) models. The aim of the present paper is to present an alternative formulation and study advantages, disadvantages, and the performance of the two formulations. In the new approach, integration of convolution integrals in the time domain is not required as before. Instead, time domain aerodynamic approximations of unsteady behavior are now cast in a form that leads, together with the equations for structural states, to second order aerodynamic equations. The resulting system of nonlinear second order equations, structural and aerodynamic, can now be solved directly using the Newton–Raphson and Newmark (Newmark, 1959) methods. Both planar and non-planar configurations are used.

2. Displacement vectors, cumulative displacement vectors, and linear unsteady aerodynamics

The displacement and cumulative displacement vectors are key quantities used in the derivations presented in this paper. The displacement vector $\boldsymbol{u}$ is relative to the configuration at the beginning of the current iteration (within a time step for the dynamic case and within a load step for the static case) in a Newton–Raphson procedure. The vector which contains the coordinates of all the structural nodes of the wing system is $\boldsymbol{x}$. The coordinates define the configuration before the displacement vector is added.

An Updated Lagrangian Formulation (Levy and Gal, 2003; Levy and Spillers, 1995; Gal and Levy, 2005) is used here and so the coordinates of the nodes are continuously updated during the iteration process.

The quantity $\boldsymbol{x}^{\alpha=0}$ represents the coordinate vector of all structural nodes at a reference aerodynamic configuration with zero angle of attack. Aerodynamic panels are defined based on the geometry of that reference configurations and structural motion away from the reference configuration is assumed small. This simplifies aerodynamic modeling in this work, since aerodynamic influence coefficients can be determined once with respect to the reference aerodynamic configuration.

The cumulative displacement vector is designated by $\boldsymbol{U}$ and is defined as the summation of all the displacements that have occurred during the iteration process up to the current iteration. Basically, the coordinates at a particular load level are obtained by adding the vector of the coordinates in the undeformed configuration ($\boldsymbol{x}^{\alpha=0}$) to the translational part of all the displacements that the structure was subjected to all the previous load levels.

The Doublet Lattice Method is used here as a representative linear unsteady aerodynamic method. Rodden's "quartic" Doublet Lattice Method (Rodden et al., 1998) is used.

3. Nonlinear structural model

The geometrically nonlinear structural model for thin-plate aerospace structures used here is created using flat triangular elements (Levy and Gal, 2003; Levy and Spillers, 1995; Gal and Levy, 2005). A tangent stiffness matrix is built for given structural shape and internal stress distributions by combining linear elastic and geometric stiffness matrices. The geometric stiffness matrix is derived by applying a load perturbation method, when the gradient (with respect to the coordinates) of the nodal force vector (when the stresses are considered fixed) is calculated. Four matrices are added to generate the geometric stiffness matrix (Levy and Gal, 2003; Levy and Spillers, 1995; Gal and Levy, 2005):

$$[\boldsymbol{K}_G^e]_{\mathrm{TOTAL}}^{\mathrm{shell}} = [\boldsymbol{K}_G^e]_{\mathrm{IP}}^{\mathrm{mem}} + [\boldsymbol{K}_G^e]_{\mathrm{IP}}^{\mathrm{plate}} + [\boldsymbol{K}_G^e]_{\mathrm{OUT}}^{\mathrm{mem}} + [\boldsymbol{K}_G^e]_{\mathrm{OUT}}^{\mathrm{plate}}. \tag{1}$$

The matrix $[\boldsymbol{K}_G^e]_{\mathrm{IP}}^{\mathrm{mem}}$, representing the in-plane contribution of a plane stress constant strain triangular element (CST), is obtained taking the gradient of the nodal forces. The matrix $[\boldsymbol{K}_G^e]_{\mathrm{IP}}^{\mathrm{plate}}$, representing the in-plane contribution of a flat triangular plate bending element, is calculated for a triangular element based on the Discrete Kirchhoff Theory (DKT). The matrix $[\boldsymbol{K}_G^e]_{\mathrm{OUT}}^{\mathrm{mem}}$, representing the out-of-plane contribution of a membrane triangular element, is calculated considering the change of a vector force which is subjected to a small rigid rotation vector $\boldsymbol{\omega}$. A similar approach is used in order to calculate the matrix $[\boldsymbol{K}_G^e]_{\mathrm{OUT}}^{\mathrm{plate}}$ which represents the out-of-plane contribution of the DKT plate element.

Rigid body motion is removed based on Levy and Gal (2003) and unbalanced loads are calculated as the nonlinear analysis (Newton–Raphson) progresses.

4. Modal-based linear unsteady aerodynamic model and full order nonlinear FEM model: full order deformation and its modal approximation

Order reduction of the structural system by using a known set of deformation shape vectors (which can be for example the natural modes of the structure or other sets of assigned shapes) is a major challenge when geometrical nonlinearities are considered. A modal basis has to be able to capture stress distributions as well as deformation shapes. The fact that the nodes are moving and can move significantly also adds to difficulty. Modal base structural order reduction methods can perform poorly when local structural behavior becomes important. When areas of important local action are known *a priori* (as in the cases of substructure synthesis, concentrated loads, etc.) special modal base vectors which can capture local action accurately in such areas can be used. But in the case of an aeroelastic system with strong geometric nonlinearity effects, location of local action of importance, such as approach of local buckling, is not known *a priori*, and, hence, reduced order models based on some general reduced basis vectors will lead to major simulation inaccuracies. The method adopted here is to use the full order structural finite element model in order to capture the nonlinear structural behavior, and to couple it with a modally reduced aerodynamic model. Such coupling covers cases in which the aerodynamic forces can be well captured by a modal approach, assuming that even with geometric structural nonlinearity effects, the overall deformation of the structure is still global in nature. Once local displacements become aerodynamically important, say, when skin panels may "pop up" locally due to local buckling, the modal approach has to be abandoned for the aerodynamics also, and a full order aerodynamic approach, with sufficient surface mesh refinement, has to be used. Such a full order approach for both structural and aerodynamic modeling will be discussed in a subsequent paper.

Details of the original formulation and the first method used for coupling nonlinear FE models with modal linear unsteady aerodynamic models can be found in Demasi and Livne (2009, 2007a). A brief summary is presented here before progression to the description of the second method.

Consider a set $\boldsymbol{\Psi}$ of $\mathscr{R}$ known shape vectors. This set can be formed by using natural modes of vibration, "fictitious mass" modes, Ritz vectors, or combinations of those (Demasi and Livne, 2007b). For the set $\boldsymbol{\Psi}$ the generalized aerodynamic matrices can be obtained by using any available linear unsteady aerodynamic simulation package (DLM, ZAERO, etc.). Such packages work in the frequency domain. That is, they provide generalized aerodynamic forces on a harmonically oscillating configuration at given reduced frequencies. Suppose we approximate the structural displacements by using the basis $\boldsymbol{\Psi}$ and the vector $\boldsymbol{q}$ of generalized coordinates as follows:

$$\boldsymbol{u} \approx \boldsymbol{\Psi}\boldsymbol{q}. \tag{2}$$

The modal approximation is focused on capturing by superposition of modes that part of the displacements that is important aerodynamically. By using a Least Square Method (LSM) it is possible to find the necessary generalized displacements as a functions of the full order displacement vector. In particular, the relation between the generalized displacements and the full order displacements is

$$\boldsymbol{q} = \boldsymbol{T}\boldsymbol{u}. \tag{3}$$

Now, the generalized aerodynamic matrices, based on the set of modes used, have to be transformed to correspond to the full order structural model. This is achieved by using work/energy conservation, and the transformation matrix is then used as will be shown in Eq. (5).

Different methods can be introduced (Demasi and Livne, 2009, 2007a, 2006) to generate $\boldsymbol{\Psi}$ and with "fictitious masses" they can lead to shapes that allow modeling refinement in desired areas or selected degrees of freedom (dofs) through the use of a modified mass matrix for the calculation of the modes. The LSM can be applied to the component of the displacements perpendicular to the wing only or to all the displacements when the modal to full order match is carried out. In particular, four modal basis were examined as follows.

(i) *Modal Basis* 1. The basis $\boldsymbol{\Psi}$ is built by using natural modes. However, the lumped mass matrix used to calculate the modes is modified by reducing the terms related to the u_x and u_y degrees of freedom by 99%. With this reduction the modes have mainly out-of-plane components in the low frequency range and the basis is more tailored to approximate the out-of-plane displacement u_z. The least squares method is performed only on the component u_z.
(ii) *Modal Basis* 2. The basis $\boldsymbol{\Psi}$ is built by using natural modes. The mass matrix is not modified. The LSM is performed only on the component u_z.
(iii) *Modal Basis* 3. The basis $\boldsymbol{\Psi}$ is built by using natural modes and the mass matrix is modified as in the case of Modal Basis 1. The LSM is performed on all the translational displacements u_x, u_y and u_z.
(iv) *Modal Basis* 4. The basis $\boldsymbol{\Psi}$ is built by using natural modes and the mass matrix is not modified as in the case of Modal Basis 2. The LSM is performed on all the translational displacements u_x, u_y and u_z. This is the method used for the most general 3-D configurations.

5. Coupling method I

The Fourier transform of the unsteady aerodynamic force corresponding to the full order structural finite element model is

$$\boldsymbol{L}_{\text{unsteady}}(\mathrm{j}\omega) = \tfrac{1}{2}\rho_\infty V_\infty^2 \boldsymbol{\mathcal{A}}_{\text{full}}(\mathrm{j}\omega)\cdot\boldsymbol{U}(\mathrm{j}\omega), \tag{4}$$

where $\boldsymbol{U}$ is the cumulative displacement vector and is a function of $\mathrm{j}\omega$ because of the time dependence of nodal positions. Cumulative displacements are used because in the present formulation the aerodynamic surface mesh is generated for the reference undeformed aerodynamic configuration, assuming that structural deformation with respect to this mesh is small enough to be within the domain of accuracy of linear aerodynamic predictions. For the unsteady case we use the same transformation from generalized coordinates to full order finite element coordinates as in the steady case (Demasi and Livne, 2009, 2007a) using the same transformation matrix $\boldsymbol{T}$. We have

$$\boldsymbol{\mathcal{A}}_{\text{full}}(\mathrm{j}\omega) = \boldsymbol{T}^{\mathrm{T}}\boldsymbol{\mathcal{A}}(\mathrm{j}\omega)\boldsymbol{T}. \tag{5}$$

The matrix $\boldsymbol{\mathcal{A}}(\mathrm{j}\omega)$ generated by an unsteady aerodynamic linear potential code is a non-rational function of the reduced frequency $k^\star = \omega b/V_\infty$: $\boldsymbol{\mathcal{A}} = \boldsymbol{\mathcal{A}}(\mathrm{j}k^\star)$. In the DLM code used for the present studies reduced frequencies were calculated based on a reference semi-chord of 1. That is, as $k = \omega/V_\infty$. A Roger procedure (Roger, 1977; Brase and Eversman, 1988) is used to obtain a rational function approximation of the generalized unsteady loads along the frequency axis. In particular, the rational function approximation is

$$\boldsymbol{\mathcal{A}}(\mathrm{j}k^\star) = \boldsymbol{\mathcal{A}}_0 + (\mathrm{j}k^\star)\boldsymbol{\mathcal{A}}_1 + (\mathrm{j}k^\star)^2\boldsymbol{\mathcal{A}}_2 + \sum_{i=1}^{N_{\text{lag}}} \frac{\mathrm{j}k^\star}{\mathrm{j}k^\star + \beta_i}\boldsymbol{\mathcal{A}}_{2+i}. \tag{6}$$

Recalling the definition of reduced frequency $k^\star$, defining $\overline{\beta}_i = (V_\infty/b)\beta_i$, simplifying and using analytical continuation to expand from the imaginary axis to the Laplace domain adjacent to it $\mathrm{j}\omega \to s$, it is possible to write the aerodynamic

generalized matrix in the Laplace domain, where s is the Laplace variable. With the help of the definitions

$$\begin{aligned}&\mathcal{A}_0^\star \doteq \tfrac{1}{2}\rho_\infty V_\infty^2 \boldsymbol{T}^{\mathrm{T}}\mathcal{A}_0\boldsymbol{T}, \quad \mathcal{A}_1^\star \doteq \tfrac{1}{2}\rho_\infty b V_\infty \boldsymbol{T}^{\mathrm{T}}\mathcal{A}_1\boldsymbol{T},\\ &\mathcal{A}_2^\star \doteq \tfrac{1}{2}\rho_\infty b^2 \boldsymbol{T}^{\mathrm{T}}\mathcal{A}_2\boldsymbol{T}, \quad \mathcal{A}_{2+i}^\star \doteq \tfrac{1}{2}\rho_\infty V_\infty^2 \boldsymbol{T}^{\mathrm{T}}\mathcal{A}_{2+i}\boldsymbol{T} \quad i=1,N_{\mathrm{lag}},\end{aligned} \tag{7}$$

the unsteady aerodynamic forces in the Laplace domain can be expressed as

$$\boldsymbol{L}_{\mathrm{unsteady}}(s) = \left[\mathcal{A}_0^\star + s\mathcal{A}_1^\star + s^2\mathcal{A}_2^\star + \sum_{i=1}^{N_{\mathrm{lag}}} \frac{s}{s+\overline{\beta}_i}\mathcal{A}_{2+\mathrm{i}}^\star\right]\boldsymbol{U}(s). \tag{8}$$

Using the Inverse Laplace Transform (ILT) expressions in the time domain can be obtained. To transform the lag terms to the time domain convolution integrals are used (Brase and Eversman, 1988). The following definitions are now introduced:

$$\mathcal{A}^\star \doteq \mathcal{A}_0^\star + \sum_{i=1}^{N_{\mathrm{lag}}} \mathcal{A}_{2+i}^\star, \tag{9}$$

$$\boldsymbol{U}(t) \doteq {}^t\boldsymbol{U}, \quad {}^t\dot{\boldsymbol{U}} \doteq \frac{\mathrm{d}[\boldsymbol{U}(t)]}{\mathrm{d}t}, \quad {}^t\ddot{\boldsymbol{U}} \doteq \frac{\mathrm{d}^2[\boldsymbol{U}(t)]}{\mathrm{d}t^2}, \quad {}^t\boldsymbol{L}_{\mathrm{unsteady}} \doteq \boldsymbol{L}_{\mathrm{unsteady}}(t). \tag{10}$$

The time domain aerodynamic forces have the following form:

$${}^t\boldsymbol{L}_{\mathrm{unsteady}} = \mathcal{A}^\star \cdot {}^t\boldsymbol{U} + \mathcal{A}_1^\star \cdot {}^t\dot{\boldsymbol{U}} + \mathcal{A}_2^\star \cdot {}^t\ddot{\boldsymbol{U}} - \sum_{i=1}^{N_{\mathrm{lag}}} \overline{\beta}_i \mathcal{A}_{2+i}^\star \int_0^t {}^\tau\boldsymbol{U}\mathrm{e}^{-\overline{\beta}_i(t-\tau)}\,\mathrm{d}\tau. \tag{11}$$

This expression for the unsteady aerodynamic loads is consistent with expressions for steady state loads (Demasi and Livne, 2009, 2007a). It involves convolution integrals that have to be evaluated to time t.

5.1. Newmark time integration and Newton–Raphson method with unsteady aerodynamics.

The equation that has to be solved at each iteration of the Newton–Raphson procedure for coupled non-aerodynamic and aerodynamic loads is (Demasi and Livne, 2009, 2007a; Bathe, 1996):

$$\boldsymbol{M}\cdot {}^{t+\Delta t}\ddot{\boldsymbol{U}}^n + \boldsymbol{C}_D \cdot {}^{t+\Delta t}\dot{\boldsymbol{U}}^n + {}^{t+\Delta t}\boldsymbol{K}_T^n \cdot {}^{t+\Delta t}\boldsymbol{u}^n = {}^{t+\Delta t}\boldsymbol{P}_{\mathrm{ext}} + {}^{t+\Delta t}\boldsymbol{L}_{\mathrm{unsteady}}^n - {}^{t+\Delta t}\boldsymbol{F}_{\mathrm{int}}^{(n-1)}, \tag{12}$$

where ${}^{t+\Delta t}\boldsymbol{L}_{\mathrm{unsteady}}^n$ is the nth realization of the aerodynamic loads at time $t+\Delta t$ and ${}^{t+\Delta t}\boldsymbol{P}_{\mathrm{ext}}$ are the external non-aerodynamic loads. Note that only the structural stiffness matrix varies with time, while the structural mass and damping matrices are constant. The explicit form of the aerodynamic force vector is (see Eq. (11))

$${}^{t+\Delta t}\boldsymbol{L}_{\mathrm{unsteady}}^n = \mathcal{A}^\star \cdot {}^{t+\Delta t}\boldsymbol{U}^n + \mathcal{A}_1^\star \cdot {}^{t+\Delta t}\dot{\boldsymbol{U}}^n + \mathcal{A}_2^\star \cdot {}^{t+\Delta t}\ddot{\boldsymbol{U}}^n - \sum_{i=1}^{N_{\mathrm{lag}}} \overline{\beta}_i \mathcal{A}_{2+i}^\star \int_0^{t+\Delta t} {}^\tau\boldsymbol{U}^n\mathrm{e}^{-\overline{\beta}_i(t+\Delta t-\tau)}\,\mathrm{d}\tau. \tag{13}$$

An important problem is the calculation of the convolution integrals in the time domain (Demasi and Livne, 2009, 2007a). A discussion of this subject is omitted here for brevity, and the reader is referred to the references for details. $\boldsymbol{C}_D$ is the full order damping matrix. In this paper a viscous damping model is used as follows. The reference generalized damping matrix is built considering a set of modes that are in general not coincident with the basis used to define the aerodynamic generalized matrices. This is done to allow direct measurement of damping ratios for a set of natural modes of a structure. Then, the reference generalized damping matrix is expanded to be of the same order of the generalized aerodynamic matrices. This operation is done by considering as a new set of modes the same modes used to define the generalized aerodynamic matrices and the transformation matrix $\boldsymbol{T}$ and by applying the least squares method to move from one set of modes to another. The generalized damping matrix is thus obtained for the same modal coordinates as the generalized aerodynamic matrix. Finally, the full order damping matrix $\boldsymbol{C}_D$ is obtained from the generalized damping matrix by using a transformation similar to Eq. (5).

5.2. Newmark's method and the iterative procedure for method I

The coupled second order nonlinear Eqs. (12) are integrated in time using the Newmark method. The adopted procedure: a mix of Newmark's integration for the structural equations and time integration of the convolution integrals is described in Demasi and Livne (2009, 2007a).

5.3. Initial conditions

To allow simulation of system response to initial perturbations initial conditions must be defined. The unsteady aerodynamic forces in the time domain are given in expression (11). If this formula is written for the initial instant $t = 0$, and setting the integrals of the lag terms to zero:

$$ {}^0\boldsymbol{L}_{\text{unsteady}} = \boldsymbol{\mathcal{A}}^{\star} \cdot {}^0\boldsymbol{U} + \boldsymbol{\mathcal{A}}_1^{\star} \cdot {}^0\dot{\boldsymbol{U}} + \boldsymbol{\mathcal{A}}_2^{\star} \cdot {}^0\ddot{\boldsymbol{U}}. \tag{14} $$

When the speed of structural nodal motions is assumed zero at $t = 0$, but allowing for initial structural acceleration or displacement,

$$ {}^0\dot{\boldsymbol{U}} = \boldsymbol{0}. \tag{15} $$

The aerodynamic force vector is then

$$ {}^0\boldsymbol{L}_{\text{unsteady}} = \boldsymbol{\mathcal{A}}^{\star} \cdot {}^0\boldsymbol{U} + \boldsymbol{\mathcal{A}}_2^{\star} \cdot {}^0\ddot{\boldsymbol{U}}. \tag{16} $$

The lag terms are still present in the aerodynamic stiffness matrix $\boldsymbol{\mathcal{A}}^{\star}$. A perturbed initial configuration $\boldsymbol{x}^{\text{pert}}$, is assumed next, for example a configuration with a small angle of attack. Thus,

$$ \boldsymbol{x}^{\text{pert}} \neq \boldsymbol{x}^{\alpha=0}. \tag{17} $$

Based on this assumption, the vectors $\boldsymbol{x}^{\text{pert}}$ and $\boldsymbol{x}^{\alpha=0}$ are augmented by adding zeros to purely rotational degrees of freedom of the structural FE model nodes (input shapes are defined by displacements only), and the vectors $\overline{\boldsymbol{x}}^{\text{pert}}$ and $\overline{\boldsymbol{x}}^{\alpha=0}$ are obtained, respectively. The cumulative displacement at the initial instant is according to the following formula:

$$ {}^0\boldsymbol{U} = \overline{\boldsymbol{x}}^{\text{pert}} - \overline{\boldsymbol{x}}^{\alpha=0}. \tag{18} $$

To find initial accelerations the equilibrium equation is written at the initial instant $t = 0$ (with structural nodal speeds zero). Then (see Eq. (12))

$$ \boldsymbol{M} \cdot {}^0\ddot{\boldsymbol{U}} = {}^0\boldsymbol{P}_{\text{ext}} + {}^0\boldsymbol{L}_{\text{unsteady}} - {}^0\boldsymbol{F}_{\text{int}}. \tag{19} $$

Assuming an initial condition that is stress free, no internal forces are present and therefore with the help of Eq. (16),

$$ \boldsymbol{M} \cdot {}^0\ddot{\boldsymbol{U}} = {}^0\boldsymbol{P}_{\text{ext}} + \boldsymbol{\mathcal{A}}^{\star} \cdot {}^0\boldsymbol{U} + \boldsymbol{\mathcal{A}}_2^{\star} \cdot {}^0\ddot{\boldsymbol{U}} \tag{20} $$

from which the initial value for the nodal accelerations can be obtained:

$$ {}^0\ddot{\boldsymbol{U}} = [\boldsymbol{M} - \boldsymbol{\mathcal{A}}_2^{\star}]^{-1} \cdot [{}^0\boldsymbol{P}_{\text{ext}} + \boldsymbol{\mathcal{A}}^{\star} \cdot {}^0\boldsymbol{U}]. \tag{21} $$

The initial conditions accepted in the present formulation can, then, account for initial deformation perturbation as well as initial force (acceleration) inputs to the system. Even when non-aerodynamic loads ($ {}^0\boldsymbol{P}_{\text{ext}} = \boldsymbol{0}$) are absent, nonzero initial accelerations due to aerodynamic initial loads can be accounted for. The time step procedure (Newmark + Newton–Raphson) can now be started with the initial conditions (15), (18) and (21) and with the initial coordinate vector $\boldsymbol{x}^{\text{pert}}$.

6. Coupled full order structural and reduced order modal aerodynamic models: method II

This new approach, presented here for the first time, avoids the need for the convolution time domain integrals of the type seen in Eq. (11).

The discussion can begin with Eq. (8). With N_{lag}, the number of lag terms, *even*, the aerodynamic forces in the Laplace domain can be rearranged as follows:

$$\boldsymbol{L}_{\text{unsteady}}(s) = [\boldsymbol{\mathcal{A}}_0^\star + s\boldsymbol{\mathcal{A}}_1^\star + s^2\boldsymbol{\mathcal{A}}_2^\star]\boldsymbol{U}(s) + \left[\sum_{i=1}^{N_{\text{lag}}/2}\left(\frac{s}{s+\overline{\beta}_{2i-1}}\boldsymbol{\mathcal{A}}_{2+(2i-1)}^\star + \frac{s}{s+\overline{\beta}_{2i}}\boldsymbol{\mathcal{A}}_{2+2i}^\star\right)\right]\boldsymbol{U}(s) \tag{22}$$

or

$$\boldsymbol{L}_{\text{unsteady}}(s) = [\boldsymbol{\mathcal{A}}_0^\star + s\boldsymbol{\mathcal{A}}_1^\star + s^2\boldsymbol{\mathcal{A}}_2^\star]\boldsymbol{U}(s) + \left[\sum_{i=1}^{N_{\text{lag}}/2}\frac{s(s+\overline{\beta}_{2i})\boldsymbol{\mathcal{A}}_{1+2i}^\star + s(s+\overline{\beta}_{2i-1})\boldsymbol{\mathcal{A}}_{2+2i}^\star}{(s+\overline{\beta}_{2i-1})(s+\overline{\beta}_{2i})}\right]\boldsymbol{U}(s). \tag{23}$$

The idea is to group the Roger lag terms in a way that will lead to aerodynamic equations in the time domain that will be of second order like the structural equations. The following definition is introduced:

$$\frac{s(s+\overline{\beta}_{2i})\boldsymbol{\mathcal{A}}_{1+2i}^\star + s(s+\overline{\beta}_{2i-1})\boldsymbol{\mathcal{A}}_{2+2i}^\star}{(s+\overline{\beta}_{2i-1})(s+\overline{\beta}_{2i})}\cdot\boldsymbol{U}(s) = \boldsymbol{\mu}_i(s). \tag{24}$$

$\boldsymbol{\mu}_i(s)$ is named *lag state variable*. There are $N_{\text{lag}}/2$ such lag state variables. The aerodynamic forces (Eq. (23)) are then rewritten in the form

$$\boldsymbol{L}_{\text{unsteady}}(s) = [\boldsymbol{\mathcal{A}}_0^\star + s\boldsymbol{\mathcal{A}}_1^\star + s^2\boldsymbol{\mathcal{A}}_2^\star]\boldsymbol{U}(s) + \sum_{i=1}^{N_{\text{lag}}/2}\boldsymbol{\mu}_i(s). \tag{25}$$

The lag state variables have to satisfy Eq. (24) which can be cast in a more convenient form:

$$s^2\boldsymbol{\mu}_i - s^2\boldsymbol{\mathcal{C}}_i\cdot\boldsymbol{U} + sB_i\boldsymbol{\mu}_i - s\boldsymbol{\mathcal{C}}_i^\star\cdot\boldsymbol{U} + B_i^\star\boldsymbol{\mu}_i = \boldsymbol{0}, \tag{26}$$

where

$$\begin{aligned} B_i &= \overline{\beta}_{2i-1} + \overline{\beta}_{2i}, \quad B_i^\star = \overline{\beta}_{2i-1}\overline{\beta}_{2i}, \\ \boldsymbol{\mathcal{C}}_i &= \boldsymbol{\mathcal{A}}_{1+2i}^\star + \boldsymbol{\mathcal{A}}_{2+2i}^\star, \quad \boldsymbol{\mathcal{C}}_i^\star = \overline{\beta}_{2i}\boldsymbol{\mathcal{A}}_{1+2i}^\star + \overline{\beta}_{2i-1}\boldsymbol{\mathcal{A}}_{2+2i}^\star. \end{aligned} \tag{27}$$

The inverse Laplace transform can now be applied to both Eqs. (26) and (25):

$$\begin{cases} {}^t\boldsymbol{L}_{\text{unsteady}} = \boldsymbol{\mathcal{A}}_2^\star\cdot{}^t\ddot{\boldsymbol{U}} + \boldsymbol{\mathcal{A}}_1^\star\cdot{}^t\dot{\boldsymbol{U}} + \boldsymbol{\mathcal{A}}_0^\star\cdot{}^t\boldsymbol{U} + \sum_{i=1}^{N_{\text{lag}}/2}{}^t\boldsymbol{\mu}_i, \\ {}^t\ddot{\boldsymbol{\mu}}_i - \boldsymbol{\mathcal{C}}_i\cdot{}^t\ddot{\boldsymbol{U}} + B_i{}^t\dot{\boldsymbol{\mu}}_i - \boldsymbol{\mathcal{C}}_i^\star\cdot{}^t\dot{\boldsymbol{U}} + B_i^\star{}^t\boldsymbol{\mu}_i = \boldsymbol{0}. \end{cases} \tag{28}$$

6.1. Newmark time integration and Newton–Raphson iterations in the case of method II

With both unsteady non-aerodynamic and aerodynamic loads and Eq. (12) the aerodynamic loads and lag state variables at time $t+\Delta t$ are obtained from Eq. (28) as follows:

$$\begin{cases} {}^{t+\Delta t}\boldsymbol{L}_{\text{unsteady}}^n = \boldsymbol{\mathcal{A}}_0^\star\cdot{}^{t+\Delta t}\boldsymbol{U}^n + \boldsymbol{\mathcal{A}}_1^\star\cdot{}^{t+\Delta t}\dot{\boldsymbol{U}}^n + \boldsymbol{\mathcal{A}}_2^\star\cdot{}^{t+\Delta t}\ddot{\boldsymbol{U}}^n + \sum_{i=1}^{N_{\text{lag}}/2}{}^{t+\Delta t}\boldsymbol{\mu}_i^n, \\ {}^{t+\Delta t}\ddot{\boldsymbol{\mu}}_i^n - \boldsymbol{\mathcal{C}}_i\cdot{}^{t+\Delta t}\ddot{\boldsymbol{U}}^n + B_i{}^{t+\Delta t}\dot{\boldsymbol{\mu}}_i^n - \boldsymbol{\mathcal{C}}_i^\star\cdot{}^{t+\Delta t}\dot{\boldsymbol{U}}^n + B_i^\star{}^{t+\Delta t}\boldsymbol{\mu}_i^n = \boldsymbol{0}, \end{cases} \tag{29}$$

with

$$i = 1, N_{\text{lag}}/2. \tag{30}$$

For Newmark's method the following quantities are defined:

$${}^{t+\Delta t}\boldsymbol{U}^n = {}^{t+\Delta t}\boldsymbol{U}_{\text{nd}}^n + {}^{t+\Delta t}\boldsymbol{u}^n, \quad {}^{t+\Delta t}\dot{\boldsymbol{U}}^n = {}^{t+\Delta t}\dot{\boldsymbol{U}}_{\text{nd}}^n + a_7a_0{}^{t+\Delta t}\boldsymbol{u}^n, \quad {}^{t+\Delta t}\ddot{\boldsymbol{U}}^n = {}^{t+\Delta t}\ddot{\boldsymbol{U}}_{\text{nd}}^n + a_0{}^{t+\Delta t}\boldsymbol{u}^n, \tag{31}$$

where

$$\begin{aligned} {}^{t+\Delta t}\boldsymbol{U}_{\text{nd}}^n &= {}^{t+\Delta t}\boldsymbol{U}^{(n-1)}, \\ {}^{t+\Delta t}\dot{\boldsymbol{U}}_{\text{nd}}^n &= {}^t\dot{\boldsymbol{U}} + a_6{}^t\ddot{\boldsymbol{U}} + a_7a_0{}^{t+\Delta t}\boldsymbol{U}^{(n-1)} - a_7a_0{}^t\boldsymbol{U} - a_7a_2{}^t\dot{\boldsymbol{U}} - a_7a_3{}^t\ddot{\boldsymbol{U}}, \\ {}^{t+\Delta t}\ddot{\boldsymbol{U}}_{\text{nd}}^n &= a_0{}^{t+\Delta t}\boldsymbol{U}^{(n-1)} - a_0{}^t\boldsymbol{U} - a_2{}^t\dot{\boldsymbol{U}} - a_3{}^t\ddot{\boldsymbol{U}}, \end{aligned} \tag{32}$$

and similarly for the lag state variables:

$$ {}^{t+\Delta t}\ddot{\boldsymbol{\mu}}_i^n = {}^{t+\Delta t}\ddot{\boldsymbol{\mu}}_{i\,\mathrm{nd}}^n + a_0\,{}^{t+\Delta t}\boldsymbol{\mu}_i^n, \quad {}^{t+\Delta t}\dot{\boldsymbol{\mu}}_i^n = {}^{t+\Delta t}\dot{\boldsymbol{\mu}}_{i\,\mathrm{nd}}^n + a_7 a_0\,{}^{t+\Delta t}\boldsymbol{\mu}_i^n, \tag{33} $$

where

$$ \begin{aligned} {}^{t+\Delta t}\ddot{\boldsymbol{\mu}}_{i\,\mathrm{nd}}^n &= -a_0\,{}^{t}\boldsymbol{\mu}_i - a_2\,{}^{t}\dot{\boldsymbol{\mu}}_i - a_3\,{}^{t}\ddot{\boldsymbol{\mu}}_i, \\ {}^{t+\Delta t}\dot{\boldsymbol{\mu}}_{i\,\mathrm{nd}}^n &= {}^{t}\dot{\boldsymbol{\mu}}_i + a_6\,{}^{t}\ddot{\boldsymbol{\mu}}_i - a_7 a_0\,{}^{t}\boldsymbol{\mu}_i - a_7 a_2\,{}^{t}\dot{\boldsymbol{\mu}}_i - a_7 a_3\,{}^{t}\ddot{\boldsymbol{\mu}}_i. \end{aligned} \tag{34} $$

Relations (31)–(34) can be substituted into Eqs. (29) and (12). It can be demonstrated that at each iteration $N_{\mathrm{lag}}/2$ equations coupled with the system of "structural" equations have to be solved. In more detail:

$$ \begin{cases} {}^{t+\Delta t}\boldsymbol{K}_{T\,\mathrm{eff}}^n \cdot \overbrace{{}^{t+\Delta t}\boldsymbol{u}^n}^{\text{unknown}} = \sum_{i=1}^{N_{\mathrm{lag}}/2} \overbrace{{}^{t+\Delta t}\boldsymbol{\mu}_i^n}^{\text{unknown}} + {}^{t+\Delta t}\boldsymbol{P}_{\mathrm{eff}}^n - {}^{t+\Delta t}\boldsymbol{F}_{\mathrm{int}}^{(n-1)}, \\ \mathcal{K}_{T\,i\,\mathrm{aero}}^{1\,\mathrm{system}} \cdot \overbrace{{}^{t+\Delta t}\boldsymbol{\mu}_i^n}^{\text{unknown}} + \mathcal{K}_{T\,i\,\mathrm{aero}}^{2\,\mathrm{system}} \cdot \overbrace{{}^{t+\Delta t}\boldsymbol{u}^n}^{\text{unknown}} = {}^{t+\Delta t}\boldsymbol{\mathcal{P}}_{i\,\mathrm{aero}}^n, \quad i = 1, N_{\mathrm{lag}}/2, \end{cases} \tag{35} $$

where

$$ \begin{aligned} &\mathcal{K}_{T\,i\,\mathrm{aero}}^{1\,\mathrm{system}} = [a_0 + a_7 a_0 B_i + B_i^\star]\boldsymbol{I} = \Omega_i \boldsymbol{I}, \quad \mathcal{K}_{T\,i\,\mathrm{aero}}^{2\,\mathrm{system}} = -a_0 \boldsymbol{\mathcal{C}}_i - a_7 a_0 \boldsymbol{\mathcal{C}}_i^\star, \\ &{}^{t+\Delta t}\boldsymbol{\mathcal{P}}_{i\,\mathrm{aero}}^n = -{}^{t+\Delta t}\ddot{\boldsymbol{\mu}}_{i\,\mathrm{nd}}^n + \boldsymbol{\mathcal{C}}_i \cdot {}^{t+\Delta t}\ddot{\boldsymbol{U}}_{\mathrm{nd}}^n - B_i \cdot {}^{t+\Delta t}\dot{\boldsymbol{\mu}}_{i\,\mathrm{nd}}^n + \boldsymbol{\mathcal{C}}_i^\star \cdot {}^{t+\Delta t}\dot{\boldsymbol{U}}_{\mathrm{nd}}^n, \\ &{}^{t+\Delta t}\boldsymbol{K}_{T\,\mathrm{eff}}^n = {}^{t+\Delta t}\boldsymbol{K}_T^n + \boldsymbol{K}_{T\,\mathrm{dyn}}^{\mathrm{system}} + \boldsymbol{K}_{T\,\mathrm{aero}}^{\mathrm{system}}, \\ &\boldsymbol{K}_{T\,\mathrm{dyn}}^{\mathrm{system}} = a_0 \boldsymbol{M} + a_7 a_0 \boldsymbol{C}_D, \quad \boldsymbol{K}_{T\,\mathrm{aero}}^{\mathrm{system}} = -\boldsymbol{\mathcal{A}}_0^\star - a_7 a_0 \boldsymbol{\mathcal{A}}_1^\star - a_0 \boldsymbol{\mathcal{A}}_2^\star, \\ &{}^{t+\Delta t}\boldsymbol{P}_{\mathrm{eff}}^n = {}^{t+\Delta t}\boldsymbol{P}_{\mathrm{ext}} + {}^{t+\Delta t}\boldsymbol{P}_{\mathrm{dyn}}^n + {}^{t+\Delta t}\boldsymbol{P}_{\mathrm{aero}}^n, \quad {}^{t+\Delta t}\boldsymbol{P}_{\mathrm{dyn}}^n = -\boldsymbol{M} \cdot {}^{t+\Delta t}\ddot{\boldsymbol{U}}_{\mathrm{nd}}^n - \boldsymbol{C}_D \cdot {}^{t+\Delta t}\dot{\boldsymbol{U}}_{\mathrm{nd}}^n, \\ &{}^{t+\Delta t}\boldsymbol{P}_{\mathrm{aero}}^n = \boldsymbol{\mathcal{A}}_0^\star \cdot {}^{t+\Delta t}\boldsymbol{U}_{\mathrm{nd}}^n + \boldsymbol{\mathcal{A}}_1^\star \cdot {}^{t+\Delta t}\dot{\boldsymbol{U}}_{\mathrm{nd}}^n + \boldsymbol{\mathcal{A}}_2^\star \cdot {}^{t+\Delta t}\ddot{\boldsymbol{U}}_{\mathrm{nd}}^n. \end{aligned} \tag{36} $$

Matrix equations condensation can now be applied to the system of Eqs. (35) with the lag state variables expressed as a function of the displacements as follows:

$$ {}^{t+\Delta t}\boldsymbol{\mu}_i^n = \frac{1}{\Omega_i}[-\mathcal{K}_{T\,i\,\mathrm{aero}}^{2\,\mathrm{system}} \cdot {}^{t+\Delta t}\boldsymbol{u}^n + {}^{t+\Delta t}\boldsymbol{\mathcal{P}}_{i\,\mathrm{aero}}^n], \quad i = 1, N_{\mathrm{lag}}/2. \tag{37} $$

Substituting into the first expression of Eq. (35):

$$ [{}^{t+\Delta t}\boldsymbol{K}_{T\,\mathrm{eff}}^n + \mathcal{K}_{T\,\mathrm{aero}}^\star] \cdot {}^{t+\Delta t}\boldsymbol{u}^n = {}^{t+\Delta t}\boldsymbol{\mathcal{P}}_{\mathrm{aero}}^{\star\,n} + {}^{t+\Delta t}\boldsymbol{P}_{\mathrm{eff}}^n - {}^{t+\Delta t}\boldsymbol{F}_{\mathrm{int}}^{(n-1)}, \tag{38} $$

where

$$ \mathcal{K}_{T\,\mathrm{aero}}^\star = \sum_{i=1}^{N_{\mathrm{lag}}/2} \left(\frac{1}{\Omega_i} \cdot \mathcal{K}_{T\,i\,\mathrm{aero}}^{2\,\mathrm{system}} \right), \quad {}^{t+\Delta t}\boldsymbol{\mathcal{P}}_{\mathrm{aero}}^{\star\,n} = \sum_{i=1}^{N_{\mathrm{lag}}/2} \left(\frac{1}{\Omega_i} \cdot {}^{t+\Delta t}\boldsymbol{\mathcal{P}}_{i\,\mathrm{aero}}^n \right). \tag{39} $$

Once the displacement ${}^{t+\Delta t}\boldsymbol{u}^n$ is found from Eq. (38), the lag state variables ${}^{t+\Delta t}\boldsymbol{\mu}_i^n$ can be obtained from Eq. (37) and the iterations can continue.

Method II presented here is completely different from Method I discussed in earlier publications. There is a restriction here to have an even number of lag terms, but calculating convolution integrals in the time domain is not necessary, and the constraint of even numbers of lag terms does not raise any problem or place any significant limitation.

$\boldsymbol{C}_D$ is the full order damping matrix and it is obtained as in Method I as explained above.

6.2. Time integration of coupled full order structural and linear modal unsteady aerodynamic equations: the full procedure

Steps of the Newmark (Bathe, 1996) method used here can now be summarized.

6.2.1. Initial calculations

First, a maximum size step is chosen by using

$$ \Delta t = \frac{T_{\min}}{N_{\text{time step}}} = \frac{2\pi b}{k_{\max}^\star V_\infty N_{\text{time step}}}; \tag{40} $$

$k^{\star}_{\max} = \omega_{\max} b / V_{\infty}$ is the maximum reduced frequency used for the Roger fit; $N_{\text{time step}}$ is a number chosen by user. If this number is larger the accuracy is improved. CPU time increases considerably, however, when $N_{\text{time step}}$ is large. The following quantities are calculated next:

$$a_0 = \frac{1}{\alpha(\Delta t)^2}, \quad a_1 = \frac{\delta}{\alpha \Delta t}, \quad a_2 = \frac{1}{\alpha \Delta t}, \quad a_3 = \frac{1}{2\alpha} - 1,$$
$$a_4 = \frac{\delta}{\alpha} - 1, \quad a_5 = \frac{\Delta t}{2}\left(\frac{\delta}{\alpha} - 2\right), \quad a_6 = \Delta t(1-\delta), \quad a_7 = \delta \Delta t, \tag{41}$$

in which $\delta = \frac{1}{2}$ and $\alpha = \frac{1}{4}$.

The parameters used in the derivation of the aerodynamic contribution are:

$$\overline{\beta}_i = \frac{V_{\infty}}{b}\beta_i, \quad B_i = \overline{\beta}_{2i-1} + \overline{\beta}_{2i}, \quad B_i^{\star} = \overline{\beta}_{2i-1}\overline{\beta}_{2i}, \quad a_0 + a_7 a_0 B_i + B_i^{\star} = \Omega_i,$$
$$\boldsymbol{\mathcal{C}}_i = \boldsymbol{\mathcal{A}}^{\star}_{1+2i} + \boldsymbol{\mathcal{A}}^{\star}_{2+2i}, \quad \boldsymbol{\mathcal{C}}_i^{\star} = \overline{\beta}_{2i}\boldsymbol{\mathcal{A}}^{\star}_{1+2i} + \overline{\beta}_{2i-1}\boldsymbol{\mathcal{A}}^{\star}_{2+2i}, \quad \mathcal{K}_{T\,i\,\text{aero}}^{2\,\text{system}} = -a_0 \boldsymbol{\mathcal{C}}_i - a_7 a_0 \boldsymbol{\mathcal{C}}_i^{\star}. \tag{42}$$

For calculation of the dynamic contribution $\boldsymbol{K}_{T\,\text{dyn}}^{\text{system}}$ to the effective tangent matrix (this contribution is constant):

$$\boldsymbol{K}_{T\,\text{dyn}}^{\text{system}} = +a_0 \boldsymbol{M} + a_7 a_0 \boldsymbol{C}_D. \tag{43}$$

Contribution to the tangent matrix due to the aerodynamic part:

$$\boldsymbol{K}_{T\,\text{aero}}^{\text{system}} = -\boldsymbol{\mathcal{A}}_0^{\star} - a_7 a_0 \boldsymbol{\mathcal{A}}_1^{\star} - a_0 \boldsymbol{\mathcal{A}}_2^{\star}. \tag{44}$$

Because of the linearity of the unsteady aerodynamic loads, this contribution does not depend on the load step or iteration and it is calculated once.

The contribution of the lag terms is

$$\mathcal{K}_{T\,\text{aero}}^{\star} = \sum_{i=1}^{N_{\text{lag}}/2}\left(\frac{1}{\Omega_i} \cdot \mathcal{K}_{T\,i\,\text{aero}}^{2\,\text{system}}\right). \tag{45}$$

This contribution also does not depend on the load step or iteration and is calculated once.

6.2.2. Time step calculations

For calculation of the external loads ${}^{t+\Delta t}\boldsymbol{P}_{\text{ext}}$ using the assigned temporal law notice that each time step defines a variation of the parameters over the interval $[t, t+\Delta t]$. The auxiliary quantities ${}^{t+\Delta t}\boldsymbol{U}_{\text{nd}}^{n}$, ${}^{t+\Delta t}\dot{\boldsymbol{U}}_{\text{nd}}^{n}$ and ${}^{t+\Delta t}\ddot{\boldsymbol{U}}_{\text{nd}}^{n}$ are calculated by using Eq. (32). This operation is performed at each iteration. If the first iteration of the current time step is considered, then the previous realization of the cumulative displacement will be ${}^{t+\Delta t}\boldsymbol{U}^{(n-1)} = {}^{t}\boldsymbol{U}$. In case the very first iteration is considered, then all the quantities are coincident with the initial (if different than zero) values. For example, ${}^{t}\boldsymbol{U} = {}^{0}\boldsymbol{U}$.

The time-step-dependent quantities ${}^{t+\Delta t}\dot{\boldsymbol{\mu}}_{i\,\text{nd}}^{n}$ and ${}^{t+\Delta t}\ddot{\boldsymbol{\mu}}_{i\,\text{nd}}^{n}$ are calculated by using Eq. (34). In the definition of the variables ${}^{t+\Delta t}\dot{\boldsymbol{\mu}}_{i\,\text{nd}}^{n}$ and ${}^{t+\Delta t}\ddot{\boldsymbol{\mu}}_{i\,\text{nd}}^{n}$ the superscript n was used as if they were dependent on the iteration, but this symbol is used only for consistency with the other variables. As a matter of fact, ${}^{t+\Delta t}\dot{\boldsymbol{\mu}}_{i\,\text{nd}}^{n}$ and ${}^{t+\Delta t}\ddot{\boldsymbol{\mu}}_{i\,\text{nd}}^{n}$ are calculated only at each time step and not at each iteration.

Next, the loads ${}^{t+\Delta t}\boldsymbol{P}_{\text{dyn}}^{n}$, ${}^{t+\Delta t}\boldsymbol{P}_{\text{aero}}^{n}$, ${}^{t+\Delta t}\boldsymbol{P}_{\text{eff}}^{n}$, ${}^{t+\Delta t}\boldsymbol{\mathcal{P}}_{i\,\text{aero}}^{n}$ and ${}^{t+\Delta t}\boldsymbol{\mathcal{P}}_{\text{aero}}^{\star\,n}$ are calculated by using Eqs. (36) and (39). The external loads ${}^{t+\Delta t}\boldsymbol{P}_{\text{ext}}$ change only when another time step is considered. Regarding the calculation of the effective tangent matrix, Eqs. (36) and (39) are used. The following linear system is then solved:

$$[{}^{t+\Delta t}\boldsymbol{K}_{T\,\text{eff}}^{n} + \mathcal{K}_{T\,\text{aero}}^{\star}] \cdot {}^{t+\Delta t}\boldsymbol{u}^{n} = {}^{t+\Delta t}\boldsymbol{\mathcal{P}}_{i\,\text{aero}}^{\star\,n} + {}^{t+\Delta t}\boldsymbol{P}_{\text{eff}}^{n} - {}^{t+\Delta t}\boldsymbol{F}_{\text{int}}^{(n-1)}. \tag{46}$$

The displacements ${}^{t+\Delta t}\boldsymbol{u}^{n}$ are used to update the coordinates of the nodes. Using the displacements ${}^{t+\Delta t}\boldsymbol{u}^{n}$ the lag state variables are calculated:

$${}^{t+\Delta t}\boldsymbol{\mu}_i^{n} = \frac{1}{\Omega_i}[-\mathcal{K}_{T\,i\,\text{aero}}^{2\,\text{system}} \cdot {}^{t+\Delta t}\boldsymbol{u}^{n} + {}^{t+\Delta t}\boldsymbol{\mathcal{P}}_{i\,\text{aero}}^{n}], \quad i = 1, N_{\text{lag}}/2. \tag{47}$$

The cumulative displacement vector is updated for the next iteration:

$${}^{t+\Delta t}\boldsymbol{U}^{n} = {}^{t+\Delta t}\boldsymbol{U}^{(n-1)} + {}^{t+\Delta t}\boldsymbol{u}^{n}. \tag{48}$$

The internal forces ${}^{t+\Delta t}\boldsymbol{F}^n_{\text{int}}$ are calculated for the next iteration. Another iteration is performed unless the convergence criteria is satisfied. If so, the iterative process in the time step is considered complete and the vectors are updated:

$$
\begin{aligned}
&{}^{t+\Delta t}\boldsymbol{U} = {}^{t+\Delta t}\boldsymbol{U}^n = {}^{t+\Delta t}\boldsymbol{U}^n_{\text{nd}} + {}^{t+\Delta t}\boldsymbol{U}^n, \quad {}^{t+\Delta t}\dot{\boldsymbol{U}} = {}^{t+\Delta t}\dot{\boldsymbol{U}}^n = {}^{t+\Delta t}\dot{\boldsymbol{U}}^n_{\text{nd}} + a_7 a_0\, {}^{t+\Delta t}\boldsymbol{u}^n,\\
&{}^{t+\Delta t}\ddot{\boldsymbol{U}} = {}^{t+\Delta t}\ddot{\boldsymbol{U}}^n = {}^{t+\Delta t}\ddot{\boldsymbol{U}}^n_{\text{nd}} + a_0\, {}^{t+\Delta t}\boldsymbol{u}^n, \quad {}^{t+\Delta t}\boldsymbol{\mu}_i = {}^{t+\Delta t}\boldsymbol{\mu}^n_i,\\
&{}^{t+\Delta t}\dot{\boldsymbol{\mu}}_i = {}^{t+\Delta t}\dot{\boldsymbol{\mu}}^n_i = {}^{t+\Delta t}\dot{\boldsymbol{\mu}}^n_{i\,\text{nd}} + a_7 a_0\, {}^{t+\Delta t}\boldsymbol{\mu}^n_i, \quad {}^{t+\Delta t}\ddot{\boldsymbol{\mu}}_i = {}^{t+\Delta t}\ddot{\boldsymbol{\mu}}^n_i = {}^{t+\Delta t}\ddot{\boldsymbol{\mu}}^n_{i\,\text{nd}} + a_0\, {}^{t+\Delta t}\boldsymbol{\mu}^n_i.
\end{aligned}
\tag{49}
$$

The process restarts with the updating of the time: $t \to t + \Delta t$.

6.3. Initial conditions

The unsteady aerodynamic forces in the time domain are given in expression (28). It is assumed that

$$
{}^0\boldsymbol{\mu}_i = {}^0\dot{\boldsymbol{\mu}}_i = \boldsymbol{0},
\tag{50}
$$

and the aerodynamic loads at the instant $t = 0$ can be written as

$$
{}^0\boldsymbol{L}_{\text{unsteady}} = \boldsymbol{\mathcal{A}}^\star_2 \cdot {}^0\ddot{\boldsymbol{U}} + \boldsymbol{\mathcal{A}}^\star_1 \cdot {}^0\dot{\boldsymbol{U}} + \boldsymbol{\mathcal{A}}^\star_0 \cdot {}^0\boldsymbol{U}.
\tag{51}
$$

As in Method I, initial structural nodal speeds are taken to be zero:

$$
{}^0\dot{\boldsymbol{U}} = \boldsymbol{0}.
\tag{52}
$$

Thus, the aerodynamic force vector is

$$
{}^0\boldsymbol{L}_{\text{unsteady}} = \boldsymbol{\mathcal{A}}^\star_2 \cdot {}^0\ddot{\boldsymbol{U}} + \boldsymbol{\mathcal{A}}^\star_0 \cdot {}^0\boldsymbol{U}.
\tag{53}
$$

Also

$$
{}^0\boldsymbol{U} = \overline{\boldsymbol{x}}^{\text{pert}} - \overline{\boldsymbol{x}}^{\alpha=0}.
\tag{54}
$$

To find the acceleration, the equilibrium equation written at the initial instant $t = 0$ is considered with structural nodal speeds zero. From Eq. (12), then

$$
\boldsymbol{M} \cdot {}^0\ddot{\boldsymbol{U}} = {}^0\boldsymbol{P}_{\text{ext}} + {}^0\boldsymbol{L}_{\text{unsteady}} - {}^0\boldsymbol{F}_{\text{int}}.
\tag{55}
$$

When the initial condition is a stress free one and no internal forces are present, then, with the help of Eq. (53),

$$
\boldsymbol{M} \cdot {}^0\ddot{\boldsymbol{U}} = {}^0\boldsymbol{P}_{\text{ext}} + \boldsymbol{\mathcal{A}}^\star_0 \cdot {}^0\boldsymbol{U} + \boldsymbol{\mathcal{A}}^\star_2 \cdot {}^0\ddot{\boldsymbol{U}}
\tag{56}
$$

from which the initial value for the acceleration can be obtained:

$$
{}^0\ddot{\boldsymbol{U}} = \left[\boldsymbol{M} - \boldsymbol{\mathcal{A}}^\star_2\right]^{-1} \cdot \left[{}^0\boldsymbol{P}_{\text{ext}} + \boldsymbol{\mathcal{A}}^\star_0 \cdot {}^0\boldsymbol{U}\right].
\tag{57}
$$

As in Method I, even in absence of non-aerodynamic loads (${}^0\boldsymbol{P}_{\text{ext}} = \boldsymbol{0}$) there can be nonzero accelerations. Initial conditions for the lag state variables have to be also defined. In Eq. (50) the lag state variables and their first time derivative are assumed to be zero. If in the second expression of Eq. (28) at time $t = 0$ ${}^0\dot{\boldsymbol{\mu}}_i = {}^0\dot{\boldsymbol{\mu}}_i = \boldsymbol{0}$ and ${}^0\dot{\boldsymbol{U}} = \boldsymbol{0}$, then

$$
{}^0\ddot{\boldsymbol{\mu}}_i - \boldsymbol{\mathcal{C}}_i \cdot {}^0\ddot{\boldsymbol{U}} = \boldsymbol{0}, \quad i = 1, N_{\text{lag}}/2,
\tag{58}
$$

or using Eq. (57),

$$
{}^0\ddot{\boldsymbol{\mu}}_i = \boldsymbol{\mathcal{C}}_i \cdot \left[\boldsymbol{M} - \boldsymbol{\mathcal{A}}^\star_2\right]^{-1} \cdot \left[{}^0\boldsymbol{P}_{\text{ext}} + \boldsymbol{\mathcal{A}}^\star_0 \cdot {}^0\boldsymbol{U}\right], \quad i = 1, N_{\text{lag}}/2.
\tag{59}
$$

The time integration procedure (Newmark + Newton−Raphson) can now be started with the initial conditions (52), (54), (57) and (59) and with the initial coordinate vector $\boldsymbol{x}^{\text{pert}}$.

7. Results

We consider the unsteady solution using the proposed methods.

7.1. First model: the delta wing

This is a well known model (Attar et al., 2005) used to capture geometric nonlinearity effects in low-aspect-ratio plate-like wings. Both numerical and experimental results are available for this model. Data for the mathematical model are as follows: 16 wing segments; 318 structural nodes, 552 structural (triangular) elements, 252 DLM aerodynamic panels, Mach = 0. The angle of attack is $\alpha = 1^\circ$.

Reduced frequencies (defined as $k^\star = \omega b/V_\infty$, where b is half-root chord) used to generate a Roger model are: 0, 0.02, 0.05, 0.1, 0.2, 0.3, 0.4, 0.5, 0.6, 0.7, 0.75, 0.8, 0.85, 0.9, 0.95, 1, 1.2, 1.4, 1.6, 1.8, 2. The selected lag terms are: $\beta_1 = 0.25$, $\beta_2 = 0.5$, $\beta_3 = 0.9$, $\beta_4 = 1.5$, $\beta_5 = 1.7$, $\beta_6 = 2.0$. The time step has to be sufficiently small for good accuracy of the results. However, it does not have to be too small to avoid excessive CPU time. $N_{\text{time step}}$ is a parameter assigned

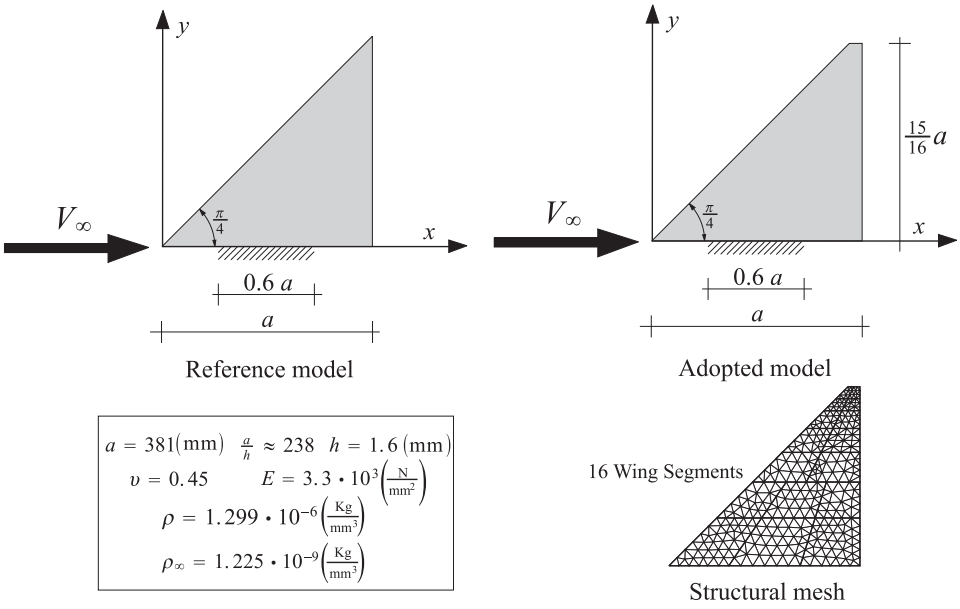

Fig. 1. The delta wing.

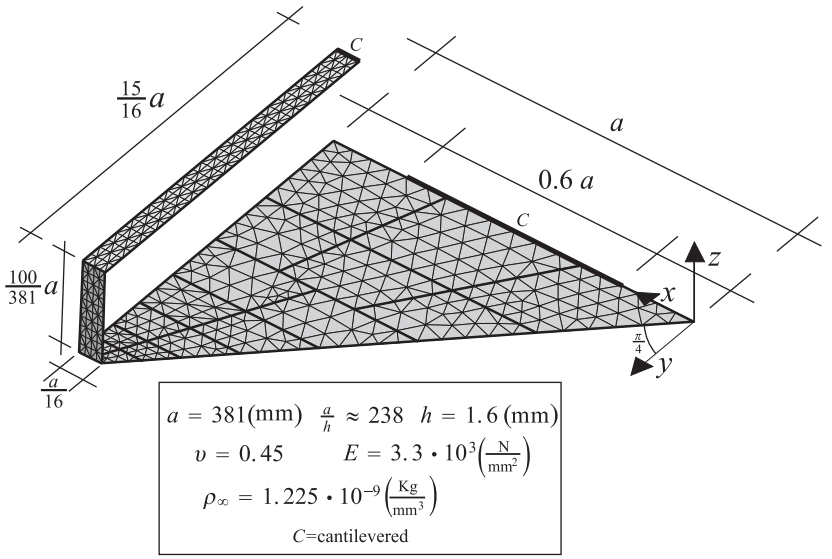

Fig. 2. Joined Wing model derived from the delta wing.

by the user (see Eq. (40)) and is used to calculate the size of the time step. Previous studies (Demasi and Livne, 2009, 2007a) have shown that it is sufficient to use $N_{\text{time step}} = 8$ and this will be adopted in all the presented cases.

7.2. Second model: the joined wing

The wing shown in Fig. 1 is modified and a Joined Wing model is created (Demasi and Livne, 2009, 2007a). The geometry of this wing is shown in Fig. 2. The wing is divided into 18 wing segments. The FE model contains 518 nodes and 872 triangular elements. The aerodynamic model contains 696 DLM panels. In all cases Mach = 0. As for the delta wing, $N_{\text{time step}} = 8$ in all cases. The angle of attack is $\alpha = 1^\circ$ on both the upper and lower wings. The angle of attack of the trapezoidal surface representing the joint is zero. This model is introduced to study the 3-D joined-wing-like effects and is directly obtained from the delta wing model. The goal is to analyze the conceptual differences between planar and non-planar cases. No practical applications of this configuration are implied.

7.3. Dynamic aeroelasticity of the delta wing: method II compared with method I

The flutter speed of this wing has been calculated numerically and experimentally validated; it is 24.5 m/s. Fig. 3 shows that at a sub-critical speed of 21 m/s excitation of the system at $t = 0$ leads to a transient that decays to converge to the steady aeroelastic solution (Demasi and Livne, 2009, 2007a) obtained by solving the nonlinear static aeroelastic problem. Twenty modes are used to generate the unsteady aerodynamic force matrices, and those 20×20 matrices and their resulting time domain Roger approximants are integrated with the full order structural FE equations. Since cantilevered modes are used for generation of the generalized aerodynamic matrices, and since the initial shape (initial angle of attack) cannot be captured by these cantilevered modes, an addition initial shape mode is added to the set of modes used for aerodynamics with DLM. Fig. 3 shows that the results obtained by using Method II for time domain simulation are slightly different than the ones obtained by using Method I. However, the simulations both converge to the same steady value (sub-critical speed: $V_\infty = 21$ m/s). When a post-flutter speed ($V_\infty = 27$ m/s) is considered, a limit cycle oscillation (LCO) is observed. Methods I and II for time domain aeroelastic simulations capture this behavior well. Figs. 4 and 5 show the LCO oscillations. Comparison with reference results is presented in Demasi and Livne (2009, 2007a). The two approaches for time domain simulations predict the same amplitudes and frequencies of LCO.

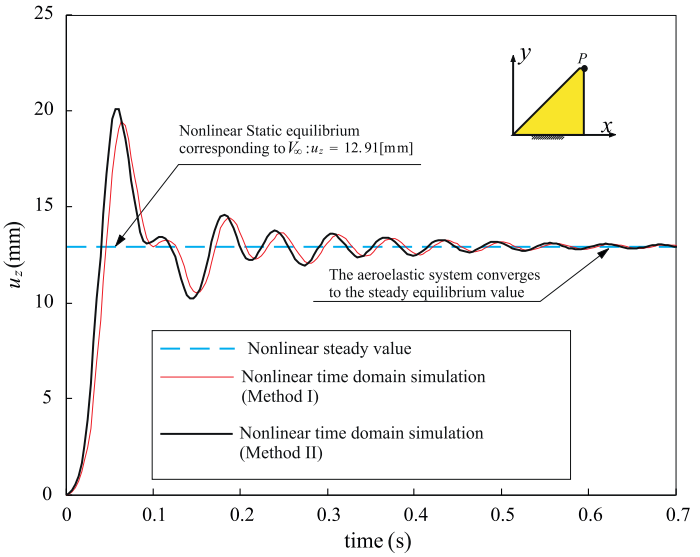

Fig. 3. Delta wing. Transient response for a sub-critical speed ($V_\infty = 21$ m/s). Time domain simulation conducted by using Methods I and II. The aerodynamic generalized matrices are approximated by using 20 modes. Six lag terms have been used. The reference damping matrix is defined by using 20 modes. Modal Basis 1 has been used and the last mode adopted for the aerodynamics has been replaced with the perturbed shape corresponding to an angle of attack $\alpha = 1^\circ$; $\zeta_i = 0.03$, $N_{\text{time step}} = 8$.

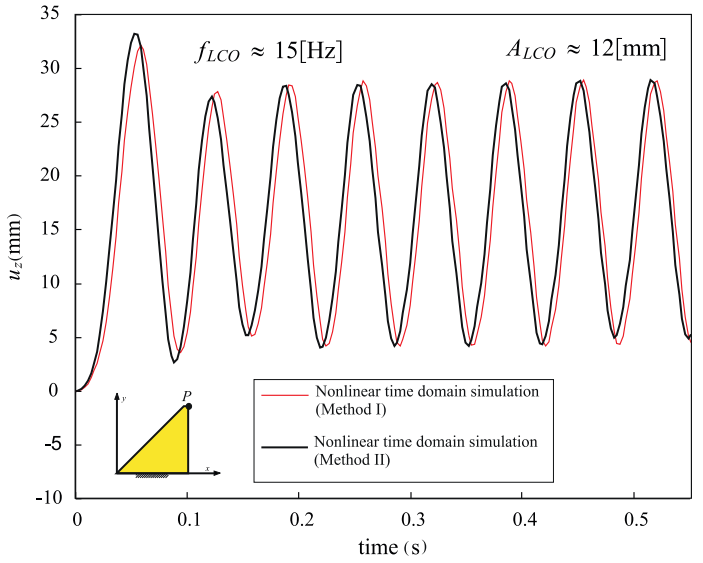

Fig. 4. Delta wing. Post-flutter LCO. $V_\infty = 27$ m/s. Time domain simulation conducted by using Methods I and II. The aerodynamic generalized matrices are approximated by using 20 modes. Six lag terms have been used. Reference damping matrix defined by using 20 modes. Modal Basis 1 has been used and the last mode adopted for the aerodynamics has been replaced with the perturbed shape corresponding to an angle of attack $\alpha = 1°$; $\zeta_i = 0.03$, $N_{\text{time step}} = 8$.

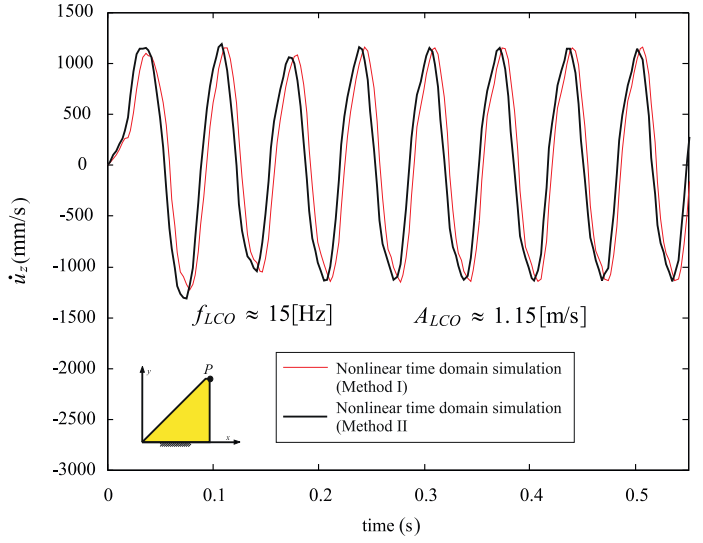

Fig. 5. Delta wing. Post-flutter LCO speed. $V_\infty = 27$ m/s. Time domain simulation conducted by using Method I and Method II. The aerodynamic generalized matrices are approximated by using 20 modes. Six lag terms have been used. Reference damping matrix defined by using 20 modes. Modal Basis 1 has been used and the last mode adopted for the aerodynamics has been replaced with the perturbed shape corresponding to an angle of attack $\alpha = 1°$; $\zeta_i = 0.03$, $N_{\text{time step}} = 8$.

7.4. Dynamic aeroelasticity of the joined wing: method II compared with method I

The present capability is valid for both planar and non-planar cases, and, actually for any 3-D configuration for which general 3-D linear unsteady aerodynamic modeling methods apply, including linearized CFD generalized aerodynamic forces (GAFs) about reference configuration shapes. Results at Mach number zero for the 3-D joined-wing configuration shown in Fig. 2 are presented in the next figure. Linear flutter speed for this configuration is 33.68 m/s. A sub-critical case is analyzed ($V_\infty = 21$ m/s). Fig. 6 shows that for that speed the convergence (after initial

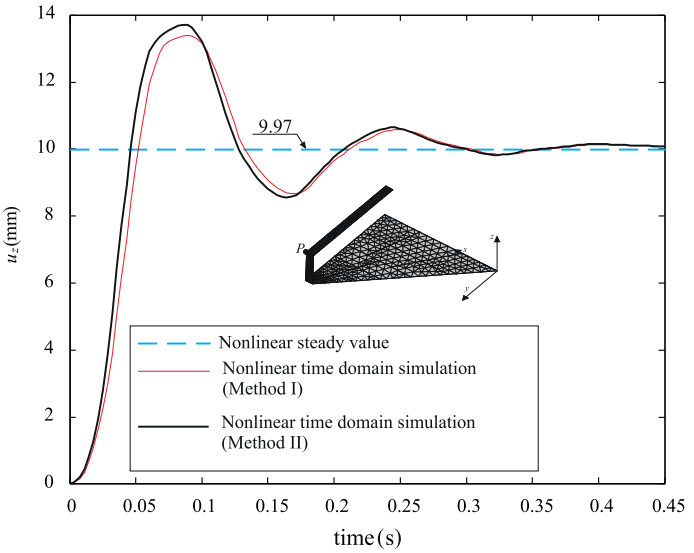

Fig. 6. Joined wing. Transient response for a sub-critical speed ($V_\infty = 21\,\mathrm{m/s}$). Time domain simulation conducted by using Methods I and II. The aerodynamic generalized matrices are approximated by using 30 modes. Six lag terms have been used. The reference damping matrix is defined by using 30 modes. Modal Basis 4 has been used and the last mode adopted for the aerodynamics has been replaced with the shape corresponding to $\alpha = 1^\circ$; $\zeta_i = 0.03$, $N_{\text{time step}} = 8$. The response is calculated at point $P \equiv a, \frac{15}{16}a, \frac{100}{381}a$. $a = 381\,\mathrm{mm}$. For this case $V_F^{\text{linear}} = 33.68\,\mathrm{m/s}$ and $f_F^{\text{linear}} = 13.06\,\mathrm{Hz}$. The linear flutter has been calculated by using 20 modes.

perturbation) to the steady state value obtained by nonlinear static aeroelastic analysis is relatively fast. Twenty modes were used to generate generalized unsteady matrices for linear flutter analysis, while 30 modes were used to generate aerodynamic matrices for the nonlinear aeroelastic cases. For the planar case (delta wing) the Methods I and II gave similar results: convergence to the steady solution for sub-critical speeds, and same frequency and amplitude for post-flutter speeds. The same happens in the non-planar JW case. However, the actual values obtained by using the two approaches are slightly different in the JW case. For example, at time $t = 7.12 \times 10^{-2}\,\mathrm{s}$ Method I gives $u_z(t)/u_{z\,\text{steady}} = 1.311$, whereas Method II gives $u_z(t)/u_{z\,\text{steady}} = 1.347$.

8. Methods I and II: a theoretical comparison

8.1. Why the two approaches give slightly different results

The two approaches have been shown to converge to the same steady solution for sub-critical cases and predict the same LCO amplitudes and frequencies for the post-flutter speed (delta wing case). But the corresponding time simulations of the two methods are not coincident. The equations on which the two approaches are based are equivalent, starting from the same equation (Eq. (8)). Method I does not introduce any auxiliary variables and leads to expression for the aerodynamic loads (Eq. (11)) which contains convolution integrals in the time domain.

Method II derivations start from the same equation in the Laplace domain (Eq. (8)), and with the introduction of auxiliary variables (the so-called lag state variables) leads to the writing of the aerodynamic loads with some auxiliary equations for the lag state variables (see in particular Eq. (28)). It is the initial conditions used to perturb the systems for a given and constant speed, as selected here, that are not mathematically equivalent. To demonstrate that consider the aerodynamic loads and the initial conditions at instant $t = 0$ for the case in which Method I is used:

$$\text{Method I} \quad \begin{cases} {}^0\boldsymbol{L}_{\text{unsteady}} = \boldsymbol{\mathcal{A}}_2^\star \cdot {}^0\ddot{\boldsymbol{U}} + \boldsymbol{\mathcal{A}}^\star \cdot {}^0\boldsymbol{U}, \\ {}^0\dot{\boldsymbol{U}} = \boldsymbol{0}, \quad {}^0\boldsymbol{U} = \overline{\boldsymbol{x}}^{\text{pert}} - \overline{\boldsymbol{x}}^{\alpha=0}, \\ {}^0\ddot{\boldsymbol{U}} = [\boldsymbol{M} - \boldsymbol{\mathcal{A}}_2^\star]^{-1} \cdot [{}^0\boldsymbol{P}_{\text{ext}} + \boldsymbol{\mathcal{A}}^\star \cdot {}^0\boldsymbol{U}]. \end{cases} \tag{60}$$

In the case of Method II the aerodynamic loads and initial conditions are

$$\text{Method II} \quad \begin{cases} {}^0\boldsymbol{L}_{\text{unsteady}} = \boldsymbol{\mathcal{A}}_2^\star \cdot {}^0\ddot{\boldsymbol{U}} + \boldsymbol{\mathcal{A}}_0^\star \cdot {}^0\boldsymbol{U}, \\ {}^0\dot{\boldsymbol{U}} = \boldsymbol{0}, \quad {}^0\boldsymbol{U} = \overline{\boldsymbol{x}}^{\text{pert}} - \overline{\boldsymbol{x}}^{\alpha=0}, \\ {}^0\ddot{\boldsymbol{U}} = [\boldsymbol{M} - \boldsymbol{\mathcal{A}}_2^\star]^{-1} \cdot [{}^0\boldsymbol{P}_{\text{ext}} + \boldsymbol{\mathcal{A}}_0^\star \cdot {}^0\boldsymbol{U}], \\ {}^0\boldsymbol{\mu}_i = {}^0\dot{\boldsymbol{\mu}}_i = \boldsymbol{0}, \quad {}^0\ddot{\boldsymbol{\mu}}_i = \boldsymbol{\mathcal{C}}_i \cdot [\boldsymbol{M} - \boldsymbol{\mathcal{A}}_2^\star]^{-1} \cdot [{}^0\boldsymbol{P}_{\text{ext}} + \boldsymbol{\mathcal{A}}_0^\star \cdot {}^0\boldsymbol{U}], \quad i = 1, N_{\text{lag}}/2. \end{cases} \tag{61}$$

The two sets of initial conditions are not identical. It is sufficient to compare the expressions of the nodal acceleration ${}^0\ddot{\boldsymbol{U}}$ at the instant $t = 0$: in one case matrix $\boldsymbol{\mathcal{A}}^\star$ is used (Method I) and in the other case matrix $\boldsymbol{\mathcal{A}}_0^\star$ is used (Method II). The two nodal initial acceleration vectors are then not identical because $\boldsymbol{\mathcal{A}}^\star \neq \boldsymbol{\mathcal{A}}_0^\star$ (see in particular Eq. (9)).

The difficulty in specifying identical initial conditions for the two methods is associated with the somewhat peculiar problem of starting the time simulations discussed here. Since the goal in linear flutter simulations is to study the dynamic behavior of the system as flight speeds are increased, the initial perturbation used to excite the system are not particularly important as long as they can excite all modes of dynamic behavior. In the nonlinear LCO case, magnitudes of initial perturbations that will lead or not lead to LCO at given speeds are important. The question is how to start the time integration of the equations at a given flight speed. In the static aeroelastic case, simulation can start at zero speed, and the speed then gradually is increased to its desired value (Demasi and Livne, 2009, 2007a). In the unsteady case, the simulation can start at zero speed, and then time stepping and speed-increases to the desired speed can be done simultaneously. This will require very long simulations. The unsteady simulation can start with the speed already set at the desired level with the system at some initial angle of attack to the flow. This means a step force input to the system (as if a wind tunnel is started suddenly at some finite dynamic pressure—the Wagner problem). Initial accelerations of the structural nodes now becomes important, and slight differences in assumptions about initial values of the unsteady aerodynamic lag states can lead to differences in the results. Methods I and II presented here seek to simplify the associated formulations regarding initial conditions for the unsteady aerodynamic lag terms, and, thus, lead to differences in the way acceleration initial conditions are accounted.

8.2. Advantages and disadvantages of the two approaches

8.2.1. Method I

With Method I $N_{\text{lag}} + 3$ aerodynamic matrices: $\boldsymbol{\mathcal{A}}^\star$, $\boldsymbol{\mathcal{A}}_1^\star$, $\boldsymbol{\mathcal{A}}_2^\star$ and the N_{lag} lag matrices $\boldsymbol{\mathcal{A}}_{2+i}^\star$ are stored and read from file (i is an index which varies from 1 to N_{lag}). When the iterations are performed, it is also necessary to continuously update the nodal variables ${}^{t+\Delta t}\boldsymbol{U}$, ${}^{t+\Delta t}\dot{\boldsymbol{U}}$ and ${}^{t+\Delta t}\ddot{\boldsymbol{U}}$ and N_{lag} auxiliary variables used for the calculation of the time domain integrals (Demasi and Livne, 2009, 2007a) indicated with ${}^{t+\Delta t}\boldsymbol{I}_i$. The aerodynamic and dynamic contributions to the effective stiffness matrix are calculated *a priori*. So, the additional matrices $\boldsymbol{K}_{T\,\text{aero}}^{\text{system}}$ and $\boldsymbol{K}_{T\,\text{dyn}}^{\text{system}}$ need to be stored. The dynamic and aerodynamic contributions (${}^{t+\Delta t}\boldsymbol{P}_{\text{dyn}}$ and ${}^{t+\Delta t}\boldsymbol{P}_{\text{aero}}$, respectively) to the applied loads need also to be updated at each iteration.

The size of the time step affects also the accuracy used in the calculation of the lag integrals.

8.2.2. Method II

There are no integrals in the time domain that have to be calculated. Unlike Method I, the number of Roger lag terms N_{lag} has to be an even number. As in Method I, with Method II $N_{\text{lag}} + 3$ aerodynamic matrices have to be stored: $\boldsymbol{\mathcal{A}}_0^\star$, $\boldsymbol{\mathcal{A}}_1^\star$, $\boldsymbol{\mathcal{A}}_2^\star$, $\boldsymbol{\mathcal{A}}_{1+2i}^\star$ and $\boldsymbol{\mathcal{A}}_{2+2i}^\star$ (notice that in the second approach it is always $i = 1, N_{\text{lag}}/2$). We need to update the nodal variables but in addition to this we need to update the lag state variables and their first and second time derivatives. More in detail, we need to update ${}^{t+\Delta t}\boldsymbol{\mu}_i$, ${}^{t+\Delta t}\dot{\boldsymbol{\mu}}_i$ and ${}^{t+\Delta t}\ddot{\boldsymbol{\mu}}_i$. But we no longer need to update the variables ${}^{t+\Delta t}\boldsymbol{I}_i$ which were used in the first approach. In addition to the quantities $\boldsymbol{K}_{T\,\text{aero}}^{\text{system}}$ and $\boldsymbol{K}_{T\,\text{dyn}}^{\text{system}}$ we also need to calculate *a priori* the matrices $\boldsymbol{\mathcal{K}}_{T\,\text{aero}}^\star$ and $\boldsymbol{\mathcal{K}}_{T\,i\,\text{aero}}^{2\,\text{system}}$. With the second approach we need to update the loads ${}^{t+\Delta t}\boldsymbol{P}_{\text{dyn}}$, ${}^{t+\Delta t}\boldsymbol{P}_{\text{aero}}$ and the new quantities ${}^{t+\Delta t}\boldsymbol{\mathcal{P}}_{i\,\text{aero}}$ and ${}^{t+\Delta t}\boldsymbol{\mathcal{P}}_{\text{aero}}^\star$. Note that with Method II the analytical expressions used for the quantities ${}^{t+\Delta t}\boldsymbol{P}_{\text{aero}}$, $\boldsymbol{K}_{T\,\text{aero}}^{\text{system}}$ are different from the corresponding quantities used in Method I for time domain simulations. More memory, then, is required with Method II to store the extra variables and matrices needed to carry out the iterative procedure.

9. Conclusion and future work

Two methods for coupling linear unsteady modally based aerodynamic codes and geometrically nonlinear FEM simulation programs have been presented. These methods allow existing linear aerodynamic panel codes (such as

doublet lattice, PANAIR, or ZAERO) to be integrated with reliable Finite Element structural capabilities such as NASTRAN or ANSYS for the analysis of wing/body configurations which portray important structural geometric nonlinearities (e.g., Joined Wings).

Method I requires the calculation of time domain integrals, whereas Method II converts unsteady aerodynamic time domain equations to second order and couples them directly with the second order structural equations. Method II does not require convolution time integrals. With Method II, however, there is an increase in computer memory required to store the extra variables needed to carry out the iterative procedure (Newton–Raphson and Newmark's method). Both Methods show excellent convergence to steady aeroelastic solutions in cases of sub-critical flight speed. When present, LCO amplitudes and frequencies calculated by using the two different approaches coincide and correlate well with experiments, in cases where experimental results exist. A decision to simplify treatment of initial conditions in the case of step variation of flight speed leads to slight differences in time histories between simulations with the two methods when a non-zero initial speed is imposed.

Modal-based generalized unsteady aerodynamic force matrices for linear aerodynamics as well as linearization of CFD loads about reference states lead to accurate prediction of aeroelastic behavior when the nature of configuration shape deformations is global and can be captured by a small set of appropriate mode shape vectors. When significant local deformation changes can appear on structural surfaces exposed to flow, such as sudden bulging of a small surface panel due to buckling or local buckling of wing areas subject to intense in-plane compression such as in joined-wing configurations, a modal approach to unsteady aerodynamics has to be abandoned and a full order approach using fine aerodynamic panel meshing has to be used. This will be the subject of a subsequent paper.

Acknowledgement

This work has been part of a University of Washington Center of Excellence on Advanced Materials in Transport Aircraft Structures (AMTAS) effort, supported by the Federal Aviation Administration, to develop simulation methods for composite airframes subject to damage and the evolution of aeroelasticity-critical nonlinear structural behavior. Peter Shyprykevich, Dr Larry Ilcewicz, and Curtis Davies, have been grant monitors. Their guidance and support are gratefully acknowledged.

References

Attar, P.J., Dowell, E.H., White, J.R., 2005. Modeling delta wing limit-cycle oscillations using a high-fidelity structural model. Journal of Aircraft 42 (5), 1209–1217.

Bathe, K.-J., 1996. Finite Element Procedures. Prentice-Hall, Englewood Cliffs, NJ, USA.

Brase, L.O., Eversman, W., 1988. Application of transient aerodynamics to the structural nonlinear flutter problem. Journal of Aircraft 25 (11), 1060–1068.

Demasi, L., Livne, E., 2006. Aeroelasticity of structurally nonlinear lifting surfaces using linear modally reduced aerodynamic generalized forces. In: 47th AIAA/ASME/ASCE/AHS/ASC Structures, Structural Dynamics and Materials Conference, Newport, RI, USA, 1–4 May.

Demasi, L., Livne, E., 2009. Dynamic aeroelasticity of structurally nonlinear configurations using linear modally reduced aerodynamic generalized forces. AIAA Journal 47 (1), 71–90.

See also: Demasi, L., Livne, E., 2007a. Dynamic aeroelasticity of structurally nonlinear configurations using linear modally reduced aerodynamic generalized forces. In: 48th AIAA/ASME/ASCE/AHS/ASC Structures, Structural Dynamics and Materials Conference, Honolulu, HI, 23–26 April.

Demasi, L., Livne, E., 2007b. The structural order reduction challenge in the case of geometrically nonlinear joined-wing configurations. In: 48th AIAA/ASME/ASCE/AHS/ASC Structures, Structural Dynamics and Materials Conference, Honolulu, HI, 23–26 April.

Friedmann, P.P., Hodges, D.H., 2003. Rotary wing aeroelasticity a historical perspective. Journal of Aircraft 40 (6), 1019–1046.

Gal, E., Levy, R., 2005. The geometric stiffness of triangular composite-materials shell elements. Computers and Structures 83, 2318–2333.

Geuzaine, P., Brown, G., Harris, C., Farhat, C., 2003. Aeroelastic dynamic analysis of a full F-16 configuration for various flight conditions. AIAA Journal 41 (3), 363–371.

Hodges, D.H., 2006. Nonlinear Composite Beam Theory. AIAA Publications.

Lee, D., Chen, P.C., 2004. Nonlinear aeroelastic studies on a joined-wing with wing buckling effects. In: AIAA-2004-1944 45th AIAA/ASME/ASCE/AHS/ASC Structures, Structural Dynamics and Materials Conference, Palm Springs, CA, April 19–22.

Levy, R., Spillers, W.R., 1995. Analysis of Geometrically Nonlinear Structures. Chapman & Hall, London.

Levy, R., Gal, E., 2003. Triangular shell element for large rotations analysis. AIAA Journal 41 (12), 2505–2508.

Livne, E., 2001. Aeroelasticity of joined-wing airplane configurations—past work and future challenges—a survey. In: AIAA Paper 2001-1370, 42nd AIAA/ASME/ASCE/AHS/ASC Structures, Structural Dynamics, and Materials Conference, Seattle, WA, USA, April 16–19.

Livne, E., Weisshaar, T.A., 2003. Aeroelasticity of nonconventional airplane configurations—past and future. Journal of Aircraft 40 (6), 1047–1065.

Newmark, N.M., 1959. A method of computation for structural dynamics. ASCE Journal of the Engineering Mechanics Division 85, 67–94.

Patil, M.J., Hodges, D.H., Cesnik, C.E.S., 2000. Nonlinear aeroelastic analysis of complete aircraft in subsonic flow. Journal of Aircraft 37 (5), 753–760.

Patil, M.J., Hodges, D.H., 2004. On the importance of aerodynamic and structural geometrical nonlinearities in aeroelastic behavior of high-aspect-ratio wings. Journal of Fluids and Structures 19 (7), 905–915.

Rodden, W.P., Taylor, P.F., McIntosh Jr., S.C., 1998. Further refinement of the subsonic doublet-lattice method. Journal of Aircraft 35 (5), 720–727.

Roger, K.L., 1977. Airplane math modeling methods for active control design. AGARD Rept. 228.

Sulaeman, E., Kapania, R., Haftka, R.T., 2002. Parametric studies of flutter speed in a strut-braced wing. In: AIAA-2002-1487 43rd AIAA/ASME/ASCE/AHS/ASC Structures, Structural Dynamics, and Materials Conference, Denver, CO, USA, April 22–25.

Tang, D.M., Dowell, E.H., 1996. Nonlinear response of a non-rotating rotor blade to a periodic gust. Journal of Fluids and Structures 10 (7), 721–742.

Tang, D., Henry, J.K., Dowell, E.H., 1999. Limit cycle oscillations of delta wing models in low subsonic flow. AIAA Journal 37 (11), 1355–1362.